Journal of Alloys and Compounds 502 (2010) 261–269

Contents lists available at ScienceDirect

Journal of Alloys and Compounds

journal homepage: www.elsevier.com/locate/jallcom

Magnetic properties of ZrNiAl-type $R_3Mn_3SiGa_2$ compounds (R = Y, Gd, Tb, Dy and Ho)

A.V. Morozkin[a,*], Lindomar Carvalho[b], R. Nirmala[c], S.K. Malik[b], O. Isnard[d,e]

[a] Department of Chemistry, Moscow State University, Leninskie Gory, House 1, Building 3, Moscow, GSP-2 119992, Russia
[b] International Center for Condensed Matter Physics—ICCMP, University of Brasilia, Brasilia 70904-970, Brazil
[c] Indian Institute of Technology Madras, Chennai 600 036, India
[d] Institut Laue-Langevin, 6 Rue J. Horowitz, 38042 Grenoble, France
[e] Institut Néel du CNRS et Université J.Fourier, BP166X, 38042 Grenoble, France

ARTICLE INFO

Article history:
Received 12 September 2009
Received in revised form
17 November 2009
Accepted 18 November 2009
Available online 24 November 2009

Keywords:
Intermetallic rare earth compounds with manganese
Magnetic measurements
Neutron diffraction
Magnetic structure

ABSTRACT

Magnetic properties of $R_3Mn_3SiGa_2$ (R = Y, Gd, Tb, Dy, Ho) compounds (hexagonal ZrNiAl-type structure; space group $P\bar{6}2m$, No.189) have been studied. Powder neutron diffraction results on $Tb_3Mn_3SiGa_2$, $Dy_3Mn_3SiGa_2$ and $Ho_3Mn_3SiGa_2$ compounds are presented. Magnetization data on $Gd_3Mn_3SiGa_2$ sample reveal a transition at about 155 K (T_N) and an anomaly at 44 K whereas the compounds with R = Tb, Dy, Ho and Y order magnetically at 125 K, 55 K, 60 K and 163 K respectively, in 0.5 T applied field. Magnetization has linear field dependence at 5 K for all these compounds. Neutron data in zero applied field reveal three magnetic transitions for $Tb_3Mn_3SiGa_2$ compound: at $T^{ND}_{m_1}\sim180$ K, $T^{ND}_{m_2} = 90$ K and $T^{ND}_{m_3} = 40$ K respectively, whereas the $Ho_3Mn_3SiGa_2$ compound shows magnetic transitions at $T^{ND}_{m_1}\sim165$ K, $T^{ND}_{m_2}\sim80$ K and $T^{ND}_{m_3} = 40$ K. Neutron diffraction study reveals that the magnetic structure is antiferromagnetic cone with wave vectors $\mathbf{K}_1 = [1/3, 1/3, 0]$, $\mathbf{K}_2 = [1/2, 1/2, 0]$ for both the compounds. The magnetic structure of $Dy_3Mn_3SiGa_2$ is also an antiferromagnetic cone but with wave vector $\mathbf{K}_2 = [1/2, 1/2, 0]$. The low temperature magnetic transition is attributed to a possible spin reorientation process.

1. Introduction

Systematic investigations are being carried out on novel ternary rare earth intermetallic phases containing manganese, in order to understand their complex magnetic properties and resulting magnetic structures. The earlier study on the magnetic properties of ZrNiAl-type RCuAl compounds [1–3] shows that these compounds order antiferromagnetically with excellent correlation between the Neél temperatures and the well-known de Gennes rule [4]. The {Gd–Ho}MnGa [5] and {Gd–Er}$MnGa_{1-x}Ge_x$ [6–8] compounds also demonstrate complex antiferromagnetic ordering. The manganese ions in these compounds have effective magnetic moments that correspond to the tetravalent, trivalent or mixed valent state of manganese ($\mu^{eff}_{Mn} = 3.6\ \mu_B$ in GdMnGa, $\mu^{eff}_{Mn} = 3.5\ \mu_B$ in TbMnGa, $\mu^{eff}_{Mn} = 3.2\ \mu_B$ in DyMnGa, $\mu^{eff}_{Mn} = 2.8\ \mu_B$ in HoMnGa [5], $\mu^{eff}_{Mn} = 4.02\ \mu_B$ in $GdMnGe_{0.5}Ga_{0.5}$ [7] and $\mu^{eff}_{Mn} = 4.4\ \mu_B$ in $TbMnGe_{0.5}Ga_{0.5}$ [8]; whereas $\mu_{Mn^{2+}} = 5.9\ \mu_B$, $\mu_{Mn^{3+}} = 5.0\ \mu_B$ and $\mu_{Mn^{4+}} = 4.0\ \mu_B$ [9]).

Due to specific features of the crystal structure in several compounds without manganese, such as ZrNiAl-type RAgGe (R = Dy, Ho, Er) [10] and TbNiAl [11] consist of square modulated magnetic moments with propagation vectors $\mathbf{K} = [1/2, 1/2, 0]$, [1/3, 1/3, 0] or [1/2, 1/2, 1/2] in their magnetic structures. The Mn-containing $R_3Mn_3GeGa_2$ compounds show high-temperature non-axial antiferromagnetic ordering that is not clearly observed in the magnetization data in low applied fields, whereas magnetic transition at low temperature coincides with the magnetic ordering temperature obtained from neutron diffraction (ND) study [12]. Recent ND measurements have resulted in better understanding of the magnetic structure of $Dy_3Mn_3SiGa_2$ compound [13].

The present work is aimed at understanding the magnetic properties of in the ZrNiAl-type rare earth compounds with manganese of RMnGa with Si substitution at Ga-site, by means of magnetization and neutron diffraction studies. The $R_3Mn_3SiGa_2$ (R = Y, Gd–Ho) compounds [14] have been prepared and characterized for this work.

2. Experimental details

The $R_3Mn_3SiGa_2$ (R = Y, Gd–Ho) compounds were prepared in an electric arc furnace under argon atmosphere using a non-consumable tungsten electrode and a water-cooled copper tray. Silicon, gallium (purity 99.99%), yttrium, gadolinium, terbium, dysprosium and holmium (purity 99.9%) and manganese (purity 99.95%) were used as starting components. Zirconium was used as a getter during melting. Subsequently, the compounds were annealed at 1070 K for 150 h in an argon atmosphere and quenched in ice-cold water.

* Corresponding author. Tel.: +7 095 9393472; fax: +7 095 9328846.
E-mail address: morozkin@general.chem.msu.ru (A.V. Morozkin).

0925-8388/$ – see front matter © 2009 Elsevier B.V. All rights reserved.
doi:10.1016/j.jallcom.2009.11.130

Table 1
Crystallographic data and magnetic properties of ZrNiAl-type $R_3Mn_3SiGa_2$ compounds (R = Y, Gd–Tm).

Compound	Unit cell data at 300 K[a]	Atomic position at 300 K[a]	R_F (%)	T_{CN}, K (0.5 T)	T_m^{ND}, K (H = 0 T)	Magnetic structure
$Y_3Mn_3SiGa_2$	a = 0.6995(1) nm c = 0.42640(5) nm	X_Y = 0.5720(7) X_{Mn} = 0.234(2)	4.1	163 7		
$Gd_3Mn_3SiGa_2$[b]	a = 0.70616(6) nm c = 0.43114(4) nm	X_{Gd} = 0.5752(3) X_{Mn} = 0.245(1)	4.2	155		
$Tb_3Mn_3SiGa_2$	a = 0.6998(1) nm	X_{Tb} = 0.5758(7)	5.5		~180	Flat spiral: non-collinear antiferromagnetic ($\mathbf{K}_1$ = [1/3, 1/3, 0] with Tb and Mn magnetic moments in *ab* plane
	c = 0.42742(7) nm	X_{Mn} = 0.246(2)				Antiferromagnetic cone: flat spiral ($\mathbf{K}_1$ = [1/3, 1/3, 0]) with antiferromagnetic component ($\mathbf{K}_2$ = [1/2, 1/2, 0]) along *c* axis and in *ab* plane
				125	90	Antiferromagnetic cone: chiefly rotation of magnetic moments along *c* axis. Flat spiral ($\mathbf{K}_1$ = [1/3, 1/3, 0] and AF component along *c* axis and in the *ab* plane ($\mathbf{K}_2$ = [1/2, 1/2, 0])
				~7	40	
$Dy_3Mn_3SiGa_2$	a = 0.6983(4) nm c = 0.4266(2) nm	X_{Dy} = 0.5752(7) X_{Mn} = 0.245(3)	6.3	55		Antiferromagnetic cone: AF component along *c* axis and in the *ab* plane ($\mathbf{K}_2$ = [1/2, 1/2, 0]). Chiefly rotation of magnetic moments along *c* axis.
$Ho_3Mn_3SiGa_2$	a = 0.6946(2) nm	X_{Ho} = 0.567(1)	6.0		165	Flat spiral: non-collinear antiferromagnetic ($\mathbf{K}_1$ = [1/3, 1/3, 0] with Tb and Mn magnetic moments in *ab* plane
	c = 0.4238(1) nm	X_{Mn} = 0.240(3)				Antiferromagnetic cone: flat spiral ($\mathbf{K}_1$ = [1/3, 1/3, 0]) with antiferromagnetic component (K_2 = [1/2, 1/2, 0]) along *c* axis and in *ab* plane
				60	90	Antiferromagnetic cone: chiefly rotation of magnetic moments along *c* axis. Flat spiral ($\mathbf{K}_1$ = [1/3, 1/3, 0] and AF component along *c* axis and in the *ab* plane ($\mathbf{K}_2$ = [1/2, 1/2, 0])
				17	40	

[a] X-ray data.
[b] crystallographic data used with permission—©JCPDS—International Centre for Diffraction Data.

X-ray powder diffraction data were obtained on an DRON-3.0 diffractometer ($Cu_{K\alpha}$-radiation, 2θ = 20–70°, step 0.05°, 1002 points). The obtained diffractograms were identified and intensity calculations in the isotropic approximation using the RIETAN-program [15].

DC magnetization data were collected using a commercial magnetometer (Physical Property Measurement System PPMS, Quantum Design, USA). For zero-field cooled (ZFC) magnetization, the sample was cooled in zero-field to 5 K and the data were acquired while warming. For the field-cold (FC) magnetization the sample was cooled in field and data were collected while warming in the same field.

The neutron diffraction experiments were performed on the powder diffractometer D1B (Institute Laue-Langevin, Grenoble, France) [16] with an incident neutron wave length λ = 0.252 nm in the temperature range 2 K < T < 200 K for various integration times. Both magnetic and crystal structures were analyzed using the FULLPROF program based on the Rietveld method [17]. The temperature at which magnetic reflections appear in the neutron diffraction pattern is taken as the magnetic transition temperature.

3. Results

3.1. Crystal structure

In the ZrNiAl-type structure, the rare earth atoms occupy the 3(g) site (X_R, 0, 1/2), manganese atoms occupy 3(f) site (X_{Mn}, 0, 0). The gallium atoms occupy the special positions 1(b) (0, 0, 1/2) and gallium and silicon atoms ($Si_{0.5}Ga_{0.5}$) occupy the special site 2(c) (1/3, 2/3, 0).

The rare earth and manganese atoms occupy the following positions in the unit cell:

$$R_j\,(j = 1,\ 2,\ 3):\ R_1\left(X_R,\ 0,\ \frac{1}{2}\right),\ R_2\left(0,\ X_R,\ \frac{1}{2}\right),$$

$$R_3\left(-X_R,\ -X_R,\ \frac{1}{2}\right);$$

$$Mn_j\,(j = 1,\ 2,\ 3):\ Mn_1\,(X_{Mn},\ 0,\ 0),\ Mn_2\,(0,\ X_{Mn},\ 0)\ \text{and}$$

$$Mn_3\,(-X_{Mn},\ -X_{Mn},\ 0).$$

The cell parameters and atomic position parameters of $R_3Mn_3SiGa_2$ compounds at room temperature are given in Table 1.

3.2. Magnetization

Magnetization of $Gd_3Mn_3SiGa_2$ has been measured as a function of temperature, in applied field of 0.5 T (Fig. 1a). This compound shows a transition at 155 K and also an anomaly at 44 K. The field dependent magnetization data obtained at 5 K indicates linear

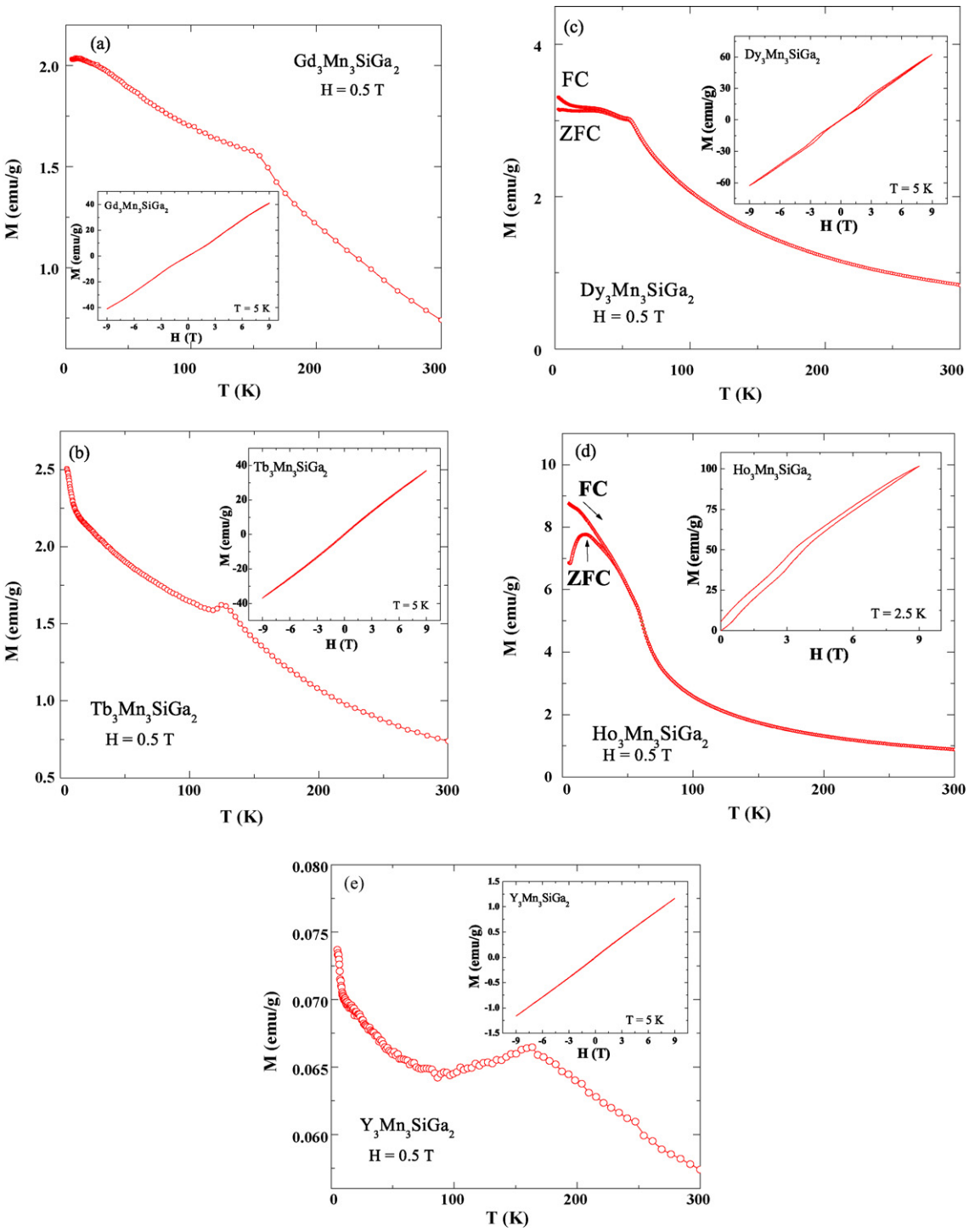

Fig. 1. (a–e) Magnetization vs temperature of $R_3Mn_3SiGa_2$ (R = Gd, Tb, Dy, Ho and Y) compounds (inset: magnetization vs field in the ordered state in fields up to 9 T).

field dependence without any hysteresis confirming the antiferromagnetic nature of this system (inset in Fig. 1a). The Tb-based compound also shows a cusp at 125 K but low temperature magnetization shows a sharp increase with a peak centred at ~7 K (Fig. 1b). The compound $Dy_3Mn_3SiGa_2$ orders magnetically at about 55 K. The zero-field cooled and field cooled magnetization data at temperatures less than T_N show mild irreversibility indicating the presence of competing magnetic interactions. Accordingly, a feeble hysteresis is noted in the field dependent magnetization data at 5 K (inset in Fig. 1c). The $Ho_3Mn_3SiGa_2$ compound undergoes a slope change in magnetization at ~60 K and shows a cusp in zero-field cooled magnetization curve at ~17 K (Fig. 1c). The difference between the ZFC and FC magnetization at low temperatures is considerably large in $Ho_3Mn_3SiGa_2$ suggesting increased ferromagnetic interactions in this system. This is further confirmed by the presence of substantial magnetic hysteresis at 2.5 K (inset in Fig. 1d) compared to the other members of this series. It is also observed that the absolute magnetization values in ordered state increases as one goes from Gd-based compound to Ho-based compound. The magnetic behaviour of non-magnetic isostructural $Y_3Mn_3SiGa_2$ sample also indicates two magnetic transitions: a cusp at ~163 K and a low temperature increase in magnetization at ~7 K (Fig. 1e).

This observation evidences the role of Mn in initiating the magnetic ordering in these compounds. The low temperature transition could be due to possible spin reorientation.

3.3. Neutron diffraction study

3.3.1. Analysis of neutron diffraction patterns (NDP)

Apriori, the set of collinear (axial) or non-axial sine modulated, flat spiral or conical spiral models (or their superposition) may be detected in complex magnetic systems such as ZrNiAl-type rare earth compounds with manganese.

The following conditions were used to determine the magnetic structure of $R_3Mn_3SiGa_2$ compounds from neutron powder diffraction data:

1. The sum of magnetic component of wave vectors in every rare earth or manganese site must correspond to the magnetic moment of rare earth in trivalent state and close to the manganese in trivalent state: $\left|\sum_{n=1,2} M(R_{ij})^{\mathbf{K}_{1,2}}\right| \leq M_{R^{3+}}$, $\left|\sum_{n=1,2} M(Mn_{ij})^{\mathbf{K}_{1,2}}\right| \leq M_{Mn^{3+}}$.
2. The magnetic structure of $R_3Mn_3SiGa_2$ must be antiferromagnetic in accordance with the present magnetic measurements.
3. Small applied magnetic fields might supress the high-temperature magnetic ordering in present compounds, as in TbNiAl [11], $Ho_3Mn_3GeGa_2$, $Er_3Mn_3GeGa_2$ and $Y_3Mn_3GeGa_2$ [12] due to non-axial magnetic ordering. For this reason the different non-collinear or flat spiral magnetic models were used for refinements of the high-temperature magnetic structure of the $Tb_3Mn_3SiGa_2$ and $Ho_3Mn_3SiGa_2$.

The following magnetic structures are most suitable from the point of view of both the neutron diffraction and magnetic data.

3.3.2. $Tb_3Mn_3SiGa_2$

Th neutron diffraction study of $Tb_3Mn_3SiGa_2$ shows appearance of new reflections at 50 K and 2 K and these correspond to the wave vectors $\mathbf{K}_1 = [1/3, 1/3, 0]$ and $\mathbf{K}_2 = [1/2, 1/2, 0]$ (Fig. 2).

The comparison of magnetic data (see Table 1) with thermal variation of neutron diffraction pattern of the $Tb_3Mn_3SiGa_2$ (Fig. 3) shows that in zero applied field the high-temperature magnetic transition occurs at $T_{m_1}^{ND}$~180 K (coincides with appearance of the (1/3, 1/3, 0) magnetic reflection), followed by the second magnetic transition at $T_{m_2}^{ND}$~90 K that corresponds to the appearance of the (1/2, 1/2 0) magnetic reflection and at $T_{m_3}^{ND}$~40 K (low temperature magnetic transition) the magnetic component with $\mathbf{K}_1 = [1/3, 1/3, 0]$ became close to constant, whereas the magnetic component with $\mathbf{K}_2 = [1/2, 1/2, 0]$ increases up to 2 K.

Below $T_{m_3}^{ND}$~40 K, the magnetic structure of $Tb_3Mn_3SiGa_2$ includes the *ab* plane antiferromagnetic component with wave vector $\mathbf{K}_1 = [1/3, 1/3, 0]$ (Tb and Mn magnetic moments lie in the basal *ab* plane) and $\mathbf{K}_2 = [1/2, 1/2, 0]$ with preferential arrangement of Tb and Mn magnetic moments along *c* axis. This magnetic structure is close to an antiferromagnetic cone. The magnetic transition at 40 K (Fig. 3) corresponds to the rotation Tb and Mn magnetic moments along *c* axis.

Between $T_{m_3}^{ND}$~40 K and $T_{m_2}^{ND}$~90 K the magnetic structure of $Tb_3Mn_3SiGa_2$ is nearly an antiferromagnetic cone again. But both AF components with wave vectors $\mathbf{K}_1$ and $\mathbf{K}_2$ increase with decreasing temperature. We may conclude that between $T_{m_2}^{ND}$~90 K and $T_{m_1}^{ND}$~180 K antiferromagnetic component with $\mathbf{K}_1 = [1/3, 1/3, 0]$ corresponds to the non-axial magnetic ordering that is given in Fig. 4a.

The images of antiferromagnetic component of $Tb_3Mn_3SiGa_2$ with $\mathbf{K}_1$ and $\mathbf{K}_2$ are given in Fig. 4a and b. The magnetic moments

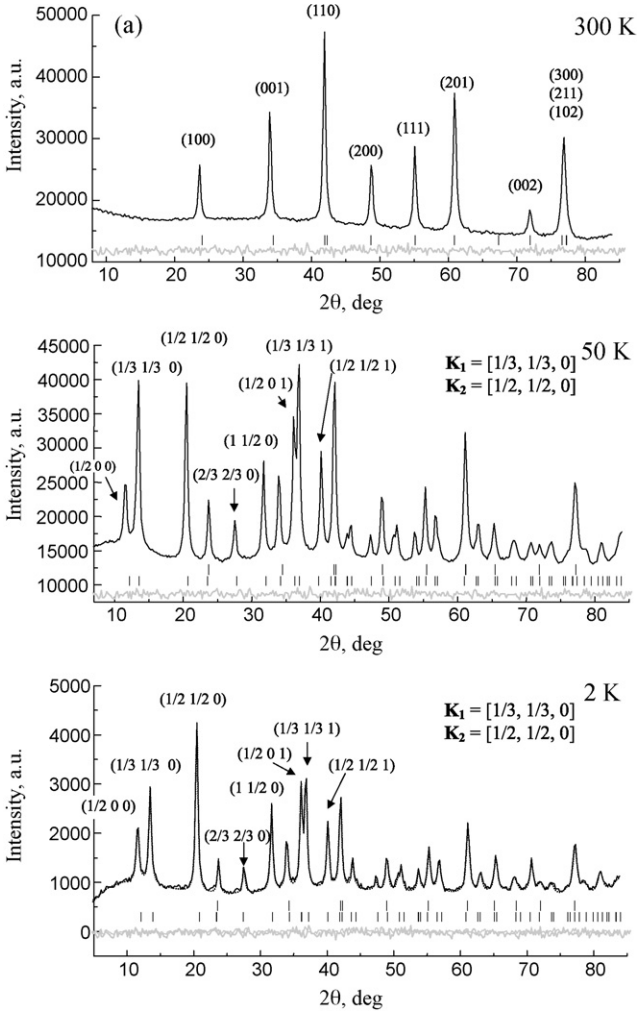

Fig. 2. Neutron diffraction patterns of $Tb_3Mn_3SiGa_2$ at 300 K (a), at 50 K (b) and at 2 K (c) (λ = 0.252 nm).

of Tb and Mn atoms in $Tb_3Mn_3SiGa_2$ are:

$$M_{Tb_j} = M_{Tb_j}^{\mathbf{K}_1} \cdot \cos\left[2\pi\left(\frac{n}{3} + \frac{m}{3}\right)\right] + M_{Tb_j}^{\mathbf{K}_2} \cdot \cos\left[2\pi\left(\frac{n}{2} + \frac{m}{2}\right)\right] \quad (n, m = 0, 1, 2\ldots)$$

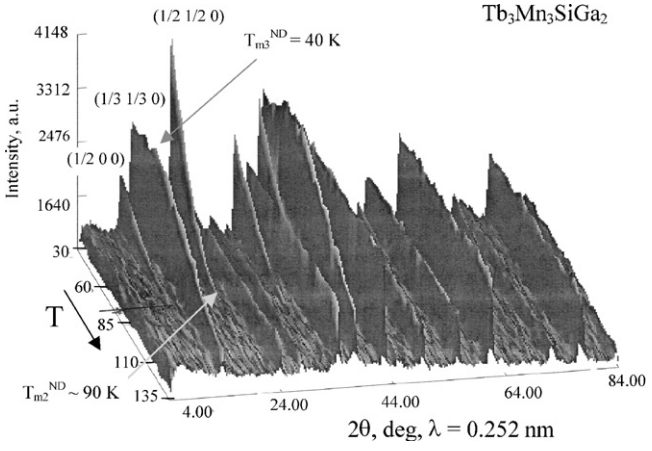

Fig. 3. Thermal variation of neutron diffraction pattern of $Tb_3Mn_3SiGa_2$.

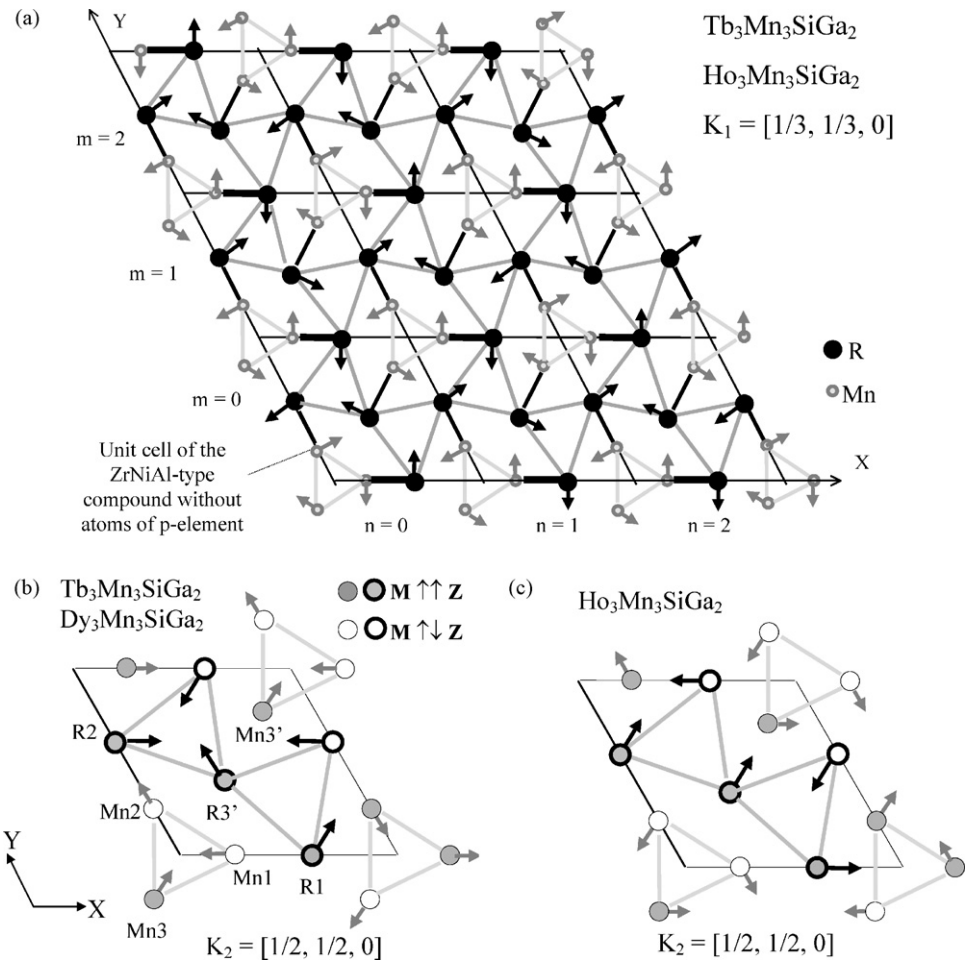

Fig. 4. Image of the antiferromagnetic component with $\mathbf{K}_1 = [1/3, 1/3, 0]$ wave vector in $Tb_3Mn_3SiGa_2$ and $Ho_3Mn_3SiGa_2$ compounds (a), the antiferromagnetic component with $\mathbf{K}_2 = [1/2, 1/2, 0]$ in $Tb_3Mn_3SiGa_2$ and $Dy_3Mn_3SiGa_2$ compounds and the antiferromagnetic component with $\mathbf{K}_2 = 1/2, 1/2, 0]$ in $Ho_3Mn_3SiGa_2$ compound (c).

$$M_{Mn_j} = M^{\mathbf{K}_1}_{Mn_j} \cdot \cos\left[2\pi\left(\frac{n}{3} + \frac{m}{3}\right)\right] + M^{\mathbf{K}_2}_{Mn_j} \cdot \cos\left[2\pi\left(\frac{n}{2} + \frac{m}{2}\right)\right] \quad (n, m = 0, 1, 2\ldots)$$

Here M_{Tb_j} and M_{Mn_j} are the magnetic moments of jth terbium and manganese atoms, respectively; $M_{Tb_j}\mathbf{K}_1$, $M_{Mn_j}\mathbf{K}_1$, $M_{Tb_j}\mathbf{K}_2$, $M_{Mn_j}\mathbf{K}_2$ are the amplitude of magnetic moment of jth terbium and manganese atoms in the magnetic sublattice with wave vectors $\mathbf{K}_1 = [1/3, 1/3, 0]$ and $\mathbf{K}_2 = [1/2, 1/2, 0]$, respectively; n and m are transition vectors along the a and b directions, respectively (see Table 2). Variation of Tb and Mn magnetic moments along a axis is plotted in Fig. 5.

3.3.3. $Dy_3Mn_3SiGa_2$

The neutron diffraction patterns of $Dy_3Mn_3SiGa_2$ down to temperature 2 K contain the magnetic reflections that corresponds to the wave vector $\mathbf{K}_2 = [1/2, 1/2, 0]$, only (Fig. 6). The corresponding magnetic structure is similar to the $Tb_3Mn_3SiGa_2$ compound (the antiferromagnetic components with $\mathbf{K}_2 = [1/2, 1/2, 0]$ of these compounds are same) (Fig. 5a). The magnetic moments of Dy and Mn atoms in $Dy_3Mn_3SiGa_2$ are:

$$M_{Dy_j} = M^{\mathbf{K}_2}_{Dy_j} \cdot \cos\left[2\pi\left(\frac{n}{2} + \frac{m}{2}\right)\right] \quad (n, m = 0, 1, 2\ldots)$$

$$M_{Mn_j} = M^{\mathbf{K}_2}_{Mn_j} \cdot \cos\left[2\pi\left(\frac{n}{2} + \frac{m}{2}\right)\right] \quad (n, m = 0, 1, 2\ldots)$$

Here M_{Dy_j} and M_{Mn_j} are the magnetic moment of jth dysprosium and manganese atoms, respectively; $M_{Dy_j}\mathbf{K}_2$, $M_{Mn_j}\mathbf{K}_2$ are the amplitude of magnetic moment of jth dysprosium and manganese atoms in the magnetic sublattice with wave vector $\mathbf{K}_2 = [1/2, 1/2, 0]$, n and m are transition vectors along the a and b axis, respectively (see Table 2).

3.3.4. $Ho_3Mn_3SiGa_2$

Th neutron diffraction study of $Ho_3Mn_3SiGa_2$ shows presence of magnetic reflections from 165 K down to 90 K that correspond to the wave vector $\mathbf{K}_1 = [1/3, 1/3, 0]$ alone (Fig. 7). Below 90 K the magnetic reflections with $\mathbf{K}_2 = [1/2, 1/2, 0]$ appear in the neutron diffraction patterns.

The comparison of magnetic data (Fig. 1) with thermal variation of intensity of the magnetic reflections of the $Ho_3Mn_3SiGa_2$ (Fig. 8) shows that in zero applied field the high-temperature magnetic transition occurs at $T^{ND}_{m_1}$~165 K (coincides with appearance of the (1/3, 1/3, 0) magnetic reflection), the second magnetic transition at $T^{ND}_{m_2}$~90 K corresponds to the appearance of the (1/2, 1/2 0) magnetic reflection and at $T^{ND}_{m_3}$~40 K the magnetic component with $\mathbf{K}_1 = [1/3, 1/3, 0]$ becomes nearly constant, whereas the magnetic component with $\mathbf{K}_2 = [1/2, 1/2, 0]$ increases down to 2 K, as in $Tb_3Mn_3SiGa_2$.

The image of the antiferromagnetic components with wave vector $\mathbf{K}_1 = [1/3, 1/3, 0]$ and $\mathbf{K}_2 = [1/2, 1/2, 0]$ is given in Fig. 4. The magnetic structure of $Ho_3Mn_3SiGa_2$ is close to the magnetic structure of $Tb_3Mn_3SiGa_2$.

Table 2
Crystallographic and magnetic parameters of ZrNiAl-type $Tb_3Mn_3SiGa_2$, $Dy_3Mn_3SiGa_2$ and $Ho_3Mn_3SiGa_2$ compounds: type of magnetic ordering (Para the paramagnetic state, AF the antiferromagnetic state), temperature of magnetic ordering from neutron diffraction experiment T^{ND}, cell parameters a and c, atomic position parameters $X_{Tb,Dy,Ho}$ and X_{Mn}, magnitude of magnetic moment of the of the corresponding atom $M_j\mathbf{K}_1$ and $M_j\mathbf{K}_2$ (μ_B) with wave vectors $\mathbf{K}_1$ and $\mathbf{K}_2$, recpectively; φ_j^{Ki} the angle (deg) with the *a* axis, the θ_j^{Ki} angle with *c* axis of the magnetic moment of corresponding atom. Reliability factors R_F (crystal structure) and R_F^m (magnetic structure) are given in percent (%).

a). $Tb_3Mn_3SiGa_2$

						$\mathbf{K}_1$ = [1/3, 1/3, 0]			$\mathbf{K}_2$ = [1/2, 1/2, 0]			
Type	T^{ND}, K	T, K	Unit cell data	R_F	Atom	$M_j\mathbf{K}_1$	$\varphi_j\mathbf{K}_1$	$\theta_j\mathbf{K}_1$	$M_j\mathbf{K}_2$	$\varphi_j\mathbf{K}_2$	$\theta_j\mathbf{K}_2$	R_F^m
Para		300[a]	a = 0.6998(2) nm c = 0.4274(1) nm X_{Tb} = 0.5758(7) X_{Mn} = 0.246(2)	5.5								
		295	a = 0.7000(2) nm c = 0.4272(2) nm X_{Tb} = 0.573(1) X_{Mn} = 0.243(5)	4.8								
AFI	$T_{m_1}^{ND}$~180	50	a = 0.6971(2) nm	4.3	Tb_1	4.9(1)	90	90	3.9(1)	60	17(4)	6.1
	$T_{m_2}^{ND}$~90		c = 0.4267(2) nm		Tb_2	4.9(1)	210	90	3.9(1)	0	17(4)	
			X_{Tb} = 0.571(2)		Tb_3	4.9(1)	330	90	3.9(1)	120	17(4)	
			X_{Mn} = 0.230(5)		Mn_1	2.1(1)	270	90	3.3(2)	180	125(3)	
					Mn_2	2.1(1)	30	90	3.3(2)	120	125(3)	
					Mn_3	2.1(1)	150	90	3.3(2)	60	55(3)	
AFII	$T_{m_2}^{ND}$~40	2	a = 0.6969(2) nm	5.0	Tb_1	5.0(1)	90	90	5.0(2)	60	11(3)	6.3
			c = 0.4267(2) nm		Tb_2	5.0(1)	210	90	5.0(2)	0	11(3)	
			X_{Tb} = 0.571(2)		Tb_3	5.0(1)	330	90	6.3(2)	120	11(3)	
			X_{Mn} = 0.240(4)		Mn_1	2.0(1)	270	90	3.7(2)	180	120(2)	
					Mn_2	2.0(1)	30	90	3.7(2)	120	120(2)	
					Mn_3	2.0(1)	150	90	3.7(2)	60	60(2)	

b). $Dy_3Mn_3SiGa_2$

					$\mathbf{K}_2$ = [1/2, 1/2, 0]			
Type	T^{ND}, K	T, K	Unit cell data	R_F	$M_j\mathbf{K}_2$	$\varphi_j\mathbf{K}_2$	$\theta_j\mathbf{K}_2$	R_F^m
Para		300[a]	a = 0.6983(4) nm c = 0.4266(2) nm X_{Dy} = 0.5711(2) X_{Mn} = 0.245(2)	6.1				
		190	a = 0.6957(2) nm c = 0.4249(2) nm X_{Dy} = 0.576(2) X_{Mn} = 0.246(6)	5.1				
AF		2	a = 0.6945(2) nm c = 0.4248(2) nm X_{Dy} = 0.573(1) X_{Mn} = 0.240(6)	4.3	6.7(2) 6.7(2) 6.7(2) 4.1(2) 4.1(2) 4.1(2)	60 0 120 180 120 60	38(2) 38(2) 38(2) 137(4) 137(4) 43(4)	6.8

(c). $Ho_3Mn_3SiGa_2$

						$\mathbf{K}_1$ = [1/3, 1/3, 0]			$\mathbf{K}_2$ = [1/2, 1/2, 0]			
Type	T^{ND}, K	T, K	Unit cell data	R_F	Atom	$M_j\mathbf{K}_1$	$\varphi_j\mathbf{K}_1$	$\theta_j\mathbf{K}_1$	$M_j\mathbf{K}_2$	$\varphi_j\mathbf{K}_2$	$\theta_j\mathbf{K}_2$	R_F^m
Para		300[a]	a = 0.6946(2) nm c = 0.4238(1) nm X_{Ho} = 0.567(1) X_{Mn} = 0.240(3)	6.0								
		194	a = 0.6955(2) nm c = 0.4243(2) nm X_{Ho} = 0.571(2) X_{Mn} = 0.243(4)	4.7								
AFI	$T_{m_1}^{ND}$~165	90	a = 0.6952(2) nm	5.6	Ho_1	3.1(1)	90	90				9.2
			c = 0.4246(2) nm		Ho_2	3.1(1)	210	90				
			X_{Ho} = 0.572(2)		Ho_3	3.1(1)	330	90				
			X_{Mn} = 0.240(5)		Mn_1	2.1(1)	270	90				
					Mn_2	2.1(1)	30	90				
					Mn_3	2.1(1)	150	90				
AFII	$T_{m_2}^{ND}$~90	50	a = 0.6933(2) nm	3.6	Ho_1	3.4(1)	90	90	4.0(2)	0	46(2)	6.1
			c = 0.4232(3) nm		Ho_2	3.4(1)	210	90	4.0(2)	60	46(2)	
			X_{Ho} = 0.570(2)		Ho_3	3.4(1)	330	90	4.0(2)	60	46(2)	
			X_{Mn} = 0.241(5)		Mn_1	1.4(1)	270	90	2.8(3)	120	127(5)	
					Mn_2	1.4(1)	30	90	2.8(3)	240	127(5)	
					Mn_3	1.4(1)	150	90	2.8(3)	0	53(5)	
AFII	$T_{m_3}^{ND}$~40	2	a = 0.6930(2) nm	3.6	Ho_1	4.4(1)	90	90	6.8(2)	0	48(2)	6.1
			c = 0.4234(2) nm		Ho_2	4.4(1)	210	90	6.8(2)	60	48(2)	
			X_{Ho} = 0.571(2)		Ho_3	4.4(1)	330	90	6.8(2)	60	48(2)	
			X_{Mn} = 0.240(4)		Mn_1	1.0(1)	270	90	3.8(3)	120	125(5)	
					Mn_2	1.0(1)	30	90	3.8(3)	240	125(5)	
					Mn_3	1.0(1)	150	90	3.8(3)	0	55(5)	

[a] X-ray data.

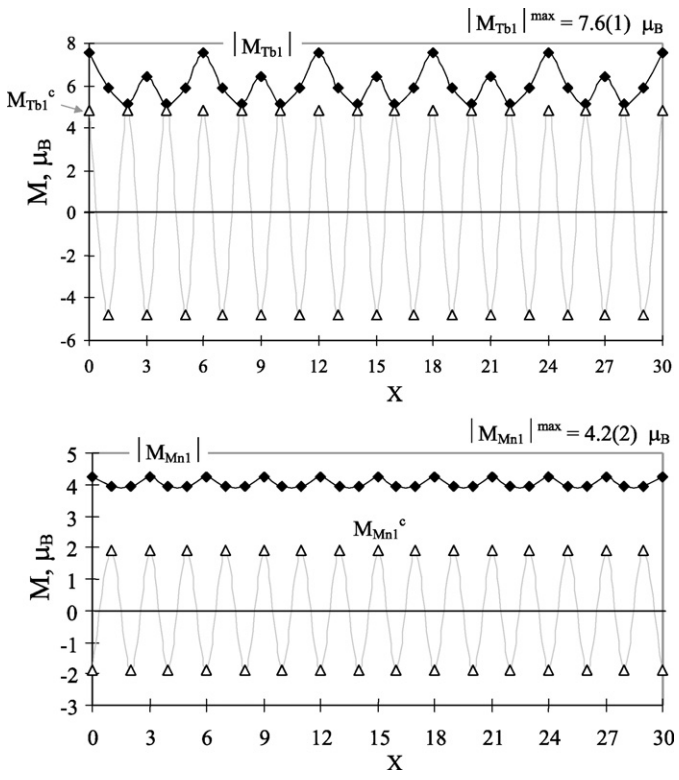

Fig. 5. Variation of terbium (a) and manganese (b) magnetic moments along *a* axis: $|M_{Tb_1}|$, $|M_{Mn_1}|$ are the magnitude of terbium and manganese magnetic moments, $|M_{Tb_1}|^c$, $|M_{Mn_1}|^c$ are the magnetic moments along *c* axis.

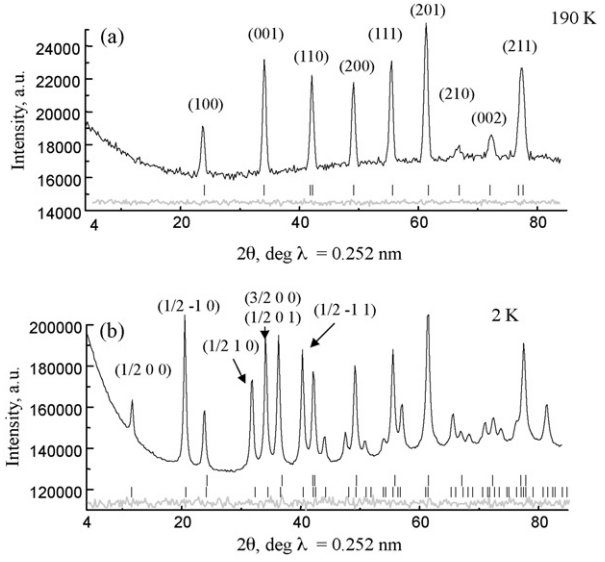

Fig. 6. Neutron diffraction patterns of $Dy_3Mn_3SiGa_2$ at temperatures 190 K and 2 K (λ = 0.252 nm).

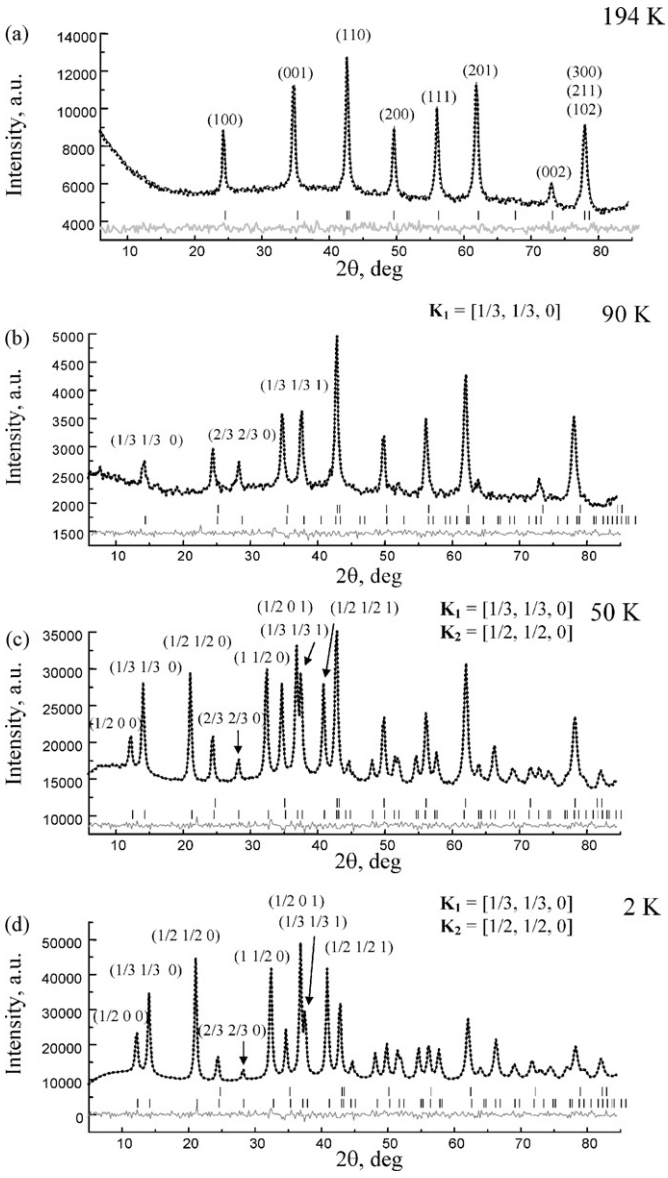

Fig. 7. Neutron diffraction patterns of $Ho_3Mn_3SiGa_2$ at temperatures 300 K (a), at 90 K (b), at 50 K (c) and at 2 K (d) (λ = 0.252 nm).

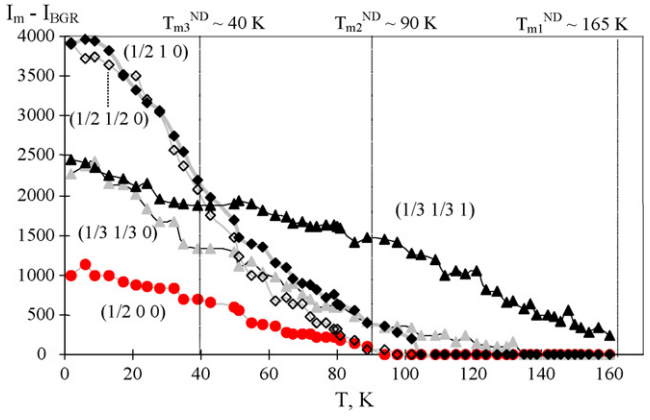

Fig. 8. Thermal variation of intensity of the magnetic reflections in neutron diffraction patterns of $Ho_3Mn_3SiGa_2$.

The magnetic moments of Ho and Mn atoms in $Ho_3Mn_3SiGa_2$ are:

$$M_{Ho_j} = M_{Ho_j}^{\mathbf{K}_1} \cdot \cos\left[2\pi\left(\frac{n}{3}+\frac{m}{3}\right)\right] + M_{Ho_j}^{\mathbf{K}_2} \cdot \cos\left[2\pi\left(\frac{n}{2}+\frac{m}{2}\right)\right] \quad (n, m = 0, 1, 2\ldots)$$

$$M_{Mn_j} = M_{Mn_j}^{\mathbf{K}_1} \cdot \cos\left[2\pi\left(\frac{n}{3}+\frac{m}{3}\right)\right] + M_{Mn_j}^{\mathbf{K}_2} \cdot \cos\left[2\pi\left(\frac{n}{2}+\frac{m}{2}\right)\right] \quad (n, m = 0, 1, 2\ldots)$$

Here M_{Ho_j} and M_{Mn_j} are the magnetic moments of jth holmium and manganese atoms, respectively; $M_{Ho_j}\mathbf{K}_1$, $M_{Mn_j}\mathbf{K}_1$, $M_{Ho_j}\mathbf{K}_2$, $M_{Mn_j}\mathbf{K}_2$ are the amplitudes of magnetic moment of jth holmium and manganese atoms in the magnetic sublattice with wave vectors $\mathbf{K}_1 = [1/3, 1/3, 0]$ and $\mathbf{K}_2 = [1/2, 1/2, 0]$, respectively; n and m are transition vectors along the a and b axis, respectively (see Table 2).

4. Discussion

The magnetic and neutron diffraction experiments show that $R_3Mn_3SiGa_2$ compounds have complex antiferromagnetic nature.

The $Tb_3Mn_3SiGa_2$ and $Dy_3Mn_3SiGa_2$ have same antiferromagnetic component with $\mathbf{K}_2 = [1/2, 1/2, 0]$ and $Tb_3Mn_3SiGa_2$ and $Ho_3Mn_3SiGa_2$ compounds have same wave vector component $\mathbf{K}_1 = [1/3, 1/3, 0]$, whereas their $\mathbf{K}_2$ component [1/2, 1/2, 0] differs.

The high-temperature magnetic ordering (as suggested by the neutron diffraction data obtained in zero magnetic field), is not observed in the magnetization data of these compounds (Fig. 1). We have observed similar low field effects in $RMnGe_{0.33}Ga_{0.66}$ [12] and Tb_5Si_3 [18] compounds. However, we observe slow increase in magnetization with decreasing temperature down to the Neèl point (Fig. 1). The T_N from magnetic measurements corresponds to the rotation of rare earth and manganese magnetic moment along c axis.

Indeed, the temperature of magnetic ordering from neutron diffraction study reflects the behavior of independent magnetic components in the sample that have different magnetic wave vectors whereas the transition temperature from magnetic measurements exhibits the overall behavior of a bulk sample and hence the magnitudes of these temperatures could differ (Table 1).

The interactions of magnetic moments of rare earth and manganese (R–R and R–Mn interactions) seem to determine the high-temperature magnetic structure in the present compounds. This interaction broadens the magnetic transition region. Of course, the peculiarity of crystal structure may also lead to an interaction of the magnetic moments of rare earth and manganese ions that facilitates the magnetic ordering. Hence magnetic transitions of the ZrNiAl-type compounds with manganese occur over a large temperature span than the ZrNiAl-type compounds without manganese.

Thus, the magnetic ordering of the ZrNiAl-type compounds with manganese has the following features:

1. High-temperature magnetic ordering may correspond to the magnetic ordering of the rare earth–manganese sublattice with arrangement of the magnetic moments in the ab plane. Due to interaction of the manganese magnetic moments with rare earth magnetic moments, the induced rare earth moment and manganese magnetic moments are collinear in the shortest R_1–Mn_1, R_2–Mn_2 and R_3–Mn_3 bond pairs (Fig. 4a).
2. The sharp increase in the magnetization may correspond to the spin reorientation of rare earth–manganese moments from basal plane to c axis and it may give rise to the low temperature anomaly in the magnetization.

Thus the magnetic manganese atoms of the ZrNiAl-type compounds seem to strongly influence the magnetic ordering temperature and magnetic structure, similar to those in TiNiSi-type TbMnGe, HoMnSi [19,20], CeFeSi-type TbMnSi, CeMnSi, PrMnSi, NdMnSi [21,22] and Fe_2P-type Er_6MnSb_2, Er_6MnBi_2 [23] and Ho_6MnBi_2 [24] compounds. In addition, the influence of the p-elements may also lead to the remarkable changes in the magnetic structures of the ZrNiAl-type compounds. The $R_3Mn_3SiGa_2$ compounds may show interesting magnetotransport properties as Tb_5Si_3 compound [18].

5. Conclusion

The Mn-containing ZrNiAl-type $R_3Mn_3SiGa_2$ (R = Y, Gd, Tb, Dy and Ho) compounds demonstrate antiferromagnetic type ordering with the complex magnetic structure. Because of structural complexity independent magnetic ordering of the manganese and rare earth sublattices is not realized in these compounds. Manganese sublattice plays an important role in triggering the magnetic transition.

Acknowledgements

This work was supported by Institute Laue-Langevin in experiments NN 5-31-1477. Thanks are due to Ouladdiaf Bachir (Institute Laue-Langeven, Grenoble, France) for his help in the experiment. Thanks to Richard Welter (Laboratoire DECOMET, Institut Le Bel, University Louis Pasteur, Strasbourg I, France) for his help in the experiment.

This work was supported by the *Russian Fund for Basic Research* through the project No. 09-03-00173-a. This work was supported by the *Indo-Russian Fund for Basic Research* through the project No. 09-03-92653-IND_a.

This work supported by a ICDD grant N 05-07. The crystallographic data of $Gd_3Mn_3SiGa_2$ used with permission—©JCPDS—International Centre for Diffraction Data.

References

[1] P. Javorsky, L. Havela, V. Sechovsky, H. Michor, K. Jurek, J. Alloys Compd. 264 (1998) 38–42.
[2] P. Javorsky, N.C. Tuan, M. Divis, L. Havela, P. Svoboda, V. Sechovsky, G. Hilscher, J. Magn. Magn. Mater. 140–144 (1995) 1139.
[3] A.V. Andreev, P. Javorsky, A. Lindbaum, J. Alloys Compd. 290 (1999) 10–16.
[4] P.G. de Gennes, C.R. Acad. Sci. (Paris) 247 (1966) 1836.
[5] J.H.V.J. Brabers, F.R. de Boer, K.H.J. Buschow, J. Alloys Compd. 179 (1992) 227–233.
[6] A.V. Morozkin, J. Alloys Compd. 352 (2003) L1–L2.
[7] T.I. Ivanova, S.A. Nikitin, A.E. Bogdanov, A.V. Morozkin, V. Suski, J.K. Warchulska, Intermetallics 13 (8) (2005) 857–861.
[8] T.I. Ivanova, S.A. Nikitin, A.E. Bogdanov, A.V. Morozkin, V. Suski, Magnetic properties and crystal structure of novel RMnGe0.5Ga0.5 compound (R = Tb, Ho), in: Novel Magnetic Materials for Microelectronic XX Conf., 12.06-16.06.2006, Moscow State Univ., Moscow, 2006, GY-22 1109-1111.
[9] S. Legvold, Rare earth metals and alloys, in: E.P. Wohlfarth (Ed.), Ferromagnetic Materials, vol. 1, North-Holland Publish. Comp., Amsterdam, 1980, pp. 183–295.
[10] S. Baran, M. Hofmann, J. Leciejewicz, B. Penc, M. Slaski, A. Szytula, J. Alloys Compd. 281 (1) (1998) 92–98.
[11] P. Javorsky, P. Burlet, V. Sechovsky, A.V. Andreev, J. Brown, P. Svoboda, J. Magn. Magn. Mater. 166 (1) (1997) 133–140.
[12] A.V. Morozkin, R. Nirmala, J. Arout Chelvane, A.K. Nigam, J. Alloys Compd. 476 (2009) 33–42.
[13] A.V. Morozkin, R. Welter, T.I. Ivanova, M.V. Makarova, O.L. Makarova, J. Alloys Compd. 415 (2006) 23–25.
[14] A.V. Morozkin, J. Alloys Compd. 363 (2004) L1–L2.
[15] F. Izumi, in: R.A. Young (Ed.), The Rietveld Method, Oxford University Press, Oxford, 1993, Chap. 13.
[16] www.ill.fr Yellow Book.
[17] J. Rodriguez-Carvajal, Physica B 192 (1993) 55–69.

[18] A.V. Morozkin, O. Isnard, R. Nirmala, S.K. Malik, J. Alloys Compd. 470 (2009) 20–23.
[19] G. Venturini, B. Malaman, E. Ressouche, J. Alloys Compd. 243 (1996) 98–105.
[20] G. Venturini, I. Ijjaali, E. Ressouche, B. Malaman, J. Alloys Compd. 256 (1997) 65–75.
[21] R. Welter, G. Venturini, E. Ressouche, B. Malaman, J. Alloys Compd. 210 (1994) 273–277.
[22] R. Welter, G. Venturini, B. Malaman, J. Alloys Compd. 206 (1994) 55–71.
[23] A.V. Morozkin, R. Nirmala, S.K. Malik, J. Alloys Compd. 394 (2005) 75–79.
[24] A.V. Morozkin, J. Alloys Compd. 395 (2005) 7–16.